JOURNAL OF CHEMICAL PHYSICS VOLUME 114, NUMBER 19 15 MAY 2001

Residual dipolar couplings between quadrupolar nuclei in solid state nuclear magnetic resonance at arbitrary fields

Sungsool Wi, Veronica Frydman, and Lucio Frydman[a]
Department of Chemistry, University of Illinois at Chicago, Chicago, Illinois 60607

(Received 30 October 2000; accepted 31 January 2001)

Second-order dipolar effects arise when a nucleus S is in close proximity to a quadrupolar spin I. These couplings originate from cross correlations between quadrupolar and dipolar interactions, and have the notable characteristic of not being susceptible to averaging by magic-angle-spinning. Therefore they can originate noticeable splittings in high resolution solid state nuclear magnetic resonance (NMR) spectra, as has been observed repeatedly for $S=1/2$. With the advent of high resolution half-integer quadrupole spectroscopy, such effects have now also been noticed in higher ($S=3/2,5/2,...$) spin systems. Within the last year these couplings have been reported for a number of complexes and analyzed in the high-field limit, when I's Larmor frequency largely exceeds its quadrupolar coupling. The present study discusses the generalization of these analyses to arbitrary quadrupolar/Zeeman ratios. The predictions of the essentially numerical treatment that results compare well with previously derived high-field analytical models, as well as with experimental solid state NMR spectra observed in a borane compound possessing a ^{11}B–^{75}As spin pair. An alternative analytical variant that can account for these effects in the low-field limit is also derived on the basis of average Hamiltonian theory; its results agree well with the predictions obtained from general numerical calculations of one-dimensional S spectra, but present peculiarities in the bi-dimensional NMR line shapes whose origins are briefly discussed. [DOI: 10.1063/1.1357440]

I. INTRODUCTION

Recent years have witnessed an increased interest in the nuclear magnetic resonance (NMR) spectroscopy of half-integer quadrupolar nuclei ($S=3/2,5/2,...$).[1–3] From a chemical perspective this interest has been driven by the large number of important roles that these nuclei play in minerals, organic and inorganic compounds, and advanced materials. Equally important have been a number of methodological advances that currently enable the acquisition of high resolution spectra from this kind of nuclei, and the exploitation of dipole-based experiments originally devised for dilute $S=1/2$ as aids in structure determination and spectral assignment. An example of one such dipole-related phenomena concerns the second-order effects that arise when a spin S is coupled to another quadrupolar nucleus I.[4,5] Cross correlations originate then between the two-spin dipolar and I's quadrupolar Hamiltonians that are not susceptible to averaging by conventional magic-angle-spinning (MAS), thereby leading to anisotropic splittings in the S-spin signal. Such residual couplings have been extensively documented in the solid state NMR spectroscopy of $S=1/2$ (^{13}C, ^{15}N, ^{31}P);[6–10] they are known to lead to unusual line shapes, as well as to information that may otherwise be difficult to extract like the sign of I's quadrupole coupling.[6–13]

With the advent of new high resolution forms of spectroscopy such as multiple-quantum magic-angle-spinning, MQMAS,[14,15] similar observations have been extended to $S=3/2$.[16–18] So far these $S-I$ residual dipole analyses have been concerned with cases where I's quadrupole coupling frequencies $\chi_Q^I=e^2qQ_I/[2I(2I-1)h]$ were small compared to their corresponding Larmor frequencies $\omega_0^I/2\pi$. It is then possible to use average Hamiltonian or perturbative methods to derive analytical expressions for the splittings and line shapes expected for the S NMR spectra, as a function of I's spin number and of the various coupling parameters involved. To deal with a more general scenario involving arbitrary values of the χ_Q^I/ω_0^I ratio, however, a different framework needs to be developed. The present study describes such arbitrary-case analysis, by introducing a numerical approach to the problem involving an explicit time propagation of the spins' density matrix. Line shapes derived in this manner for a model $I=S=3/2$ spin system agreed well with the predictions of our previous analytical theories in the high field limit, and allowed us to test the latter's applicability range. The numerical procedure was also used to follow the high→intermediate-field transition of this effect, as monitored experimentally via ^{11}B MQMAS NMR on a ^{11}B–^{75}As spin pair as a function of the magnetic field strength. Finally, these numerical simulations were complemented with an analytical low-field theory derived to account for the consequences of these effects in the $\omega_0^I \ll \chi_Q^I$ regime. The similarities and discrepancies observed between this analytical theory and the numerical predictions of the general model are discussed.

---

[a] Author to whom correspondence should be addressed. Department of Chemical Physics, Weizmann Institute of Sciences, 76100 Rehovot, Israel. Electronic mail: lucio.frydman@weizmann.weizmann.ac.il

II. RESIDUAL DIPOLAR COUPLINGS AT ARBITRARY FIELDS

In deriving a general approach for analyzing quadrupole-induced dipolar effects under arbitrary χ_Q^I/ω_0^I conditions, we decided to follow the general outline and nomenclature laid out in our previous high-field analysis.[18] Furthermore, since the focus of the present work is an $I-S$ pair where S is observed under high-field/high-resolution conditions while I's Hamiltonian is dominated by a quadrupole interaction, only heteronuclear systems had to be considered. Hence, the total laboratory frame Hamiltonian can be written as

$$\mathcal{H}_{\rm Lab}=\mathcal{H}_Z^I+\mathcal{H}_Z^S+\mathcal{H}_Q^I+\mathcal{H}_Q^S+\mathcal{H}_{IS}. \tag{1}$$

Here

$$\mathcal{H}_Z^X=\frac{\omega_0^X}{2\pi}X_z, \quad X=I,S, \tag{2a}$$

$$\mathcal{H}_Q^X=\sum_{m=-2}^{2}(-I)^m T_{2,-m}^{Q,X}R_{2,m}^{Q,X}, \quad X,I,S, \tag{2b}$$

and

$$\mathcal{H}_{IS}=\mathcal{H}_{IS}^D+\mathcal{H}_{IS}^J=J\overline{I}\cdot\overline{S}+\sum_{m=-2}^{2}(-I)^m T_{2,-m}^{D}R_{2,m}^{D_{\rm eff}} \tag{2c}$$

denote, respectively, the Zeeman, quadrupolar, and $I-S$ coupling interactions of the two spins in terms irreducible spherical tensor components.[19] Moreover, the last of these interactions considers J and dipolar couplings in unison by assuming that they possess coincident principal axis systems (PASs), and are therefore defined by a net anisotropic constant $D_{zz}^{\rm eff}=-2(\gamma_I\gamma_S\hbar r_{IS}^{-3}-\Delta J/3)$.[20]

Because of our interest in the high resolution spectroscopy of S under MAS and MQMAS conditions, it is sensible to assume that $\omega_0^S/2\pi \gg \chi_Q^S=e^2qQ/[2S(2S-1)h]$. S Zeeman effects can then be accounted by the customary rotating frame transformation $\tilde{\mathcal{H}}_{\rm Lab}(t)=e^{i\omega_0^S S_z t}\mathcal{H}_{\rm Lab}e^{-i\omega_0^S S_z t}$, followed by an average Hamiltonian treatment to account for the time dependencies imparted on the spin operators. The resulting rotating frame Hamiltonian can be written as

$$\begin{aligned}\mathcal{H}_{\rm rot}&=\mathcal{H}_I+\mathcal{H}_S+\mathcal{H}_{IS}\\&=(\mathcal{H}_Z^I+\mathcal{H}_Q^I)+(\delta_S S_z+\mathcal{H}_S^{Q,(1)}+\mathcal{H}_S^{Q,(2)})+\mathcal{H}_{IS}^{(1)}.\end{aligned} \tag{3}$$

In this expression the $\mathcal{H}_I$ terms are as in Eqs. (2a) and (2b), δ_S is a frequency offset, $\mathcal{H}_S^{Q,(1,2)}$ are S's first- and second-order quadrupole effects, and $\mathcal{H}_{IS}^{(I)}$ represents the dipolar effects truncated to first order in S_z:

$$\mathcal{H}_{IS}^{(1)}=\left(J+\sqrt{\frac{2}{3}}R_{2,0}^{D_{\rm eff}}\right)I_zS_z+\frac{1}{2}(R_{2,-1}^{D_{\rm eff}}I_+-R_{2,1}^{D_{\rm eff}}I_-)S_z. \tag{4}$$

The first term on the right-hand side of this equation represents the secular heteronuclear $I-S$ coupling, whereas the second one contains the nonsecular effects that constitute the focus of this study.

Previous analyses assumed that both S and I were subject to high-field conditions, and thus continued at this point with a rotating-frame I transformation similar to the one applied on S. Yet for arbitrary χ_Q^I/ω_0^I ratios such transformation is no longer justified, and an explicit diagonalization of the Hamiltonian needs to be carried out for evaluating the spectra. In order to specify the form of this matrix we circumscribed the analysis to $S=I=3/2$, coinciding with the type of spin system that was subsequently analyzed experimentally. The $\mathcal{H}_{\rm rot}$ operator in the product $\{|m_S m_I\rangle\}$ Zeeman basis set then reads

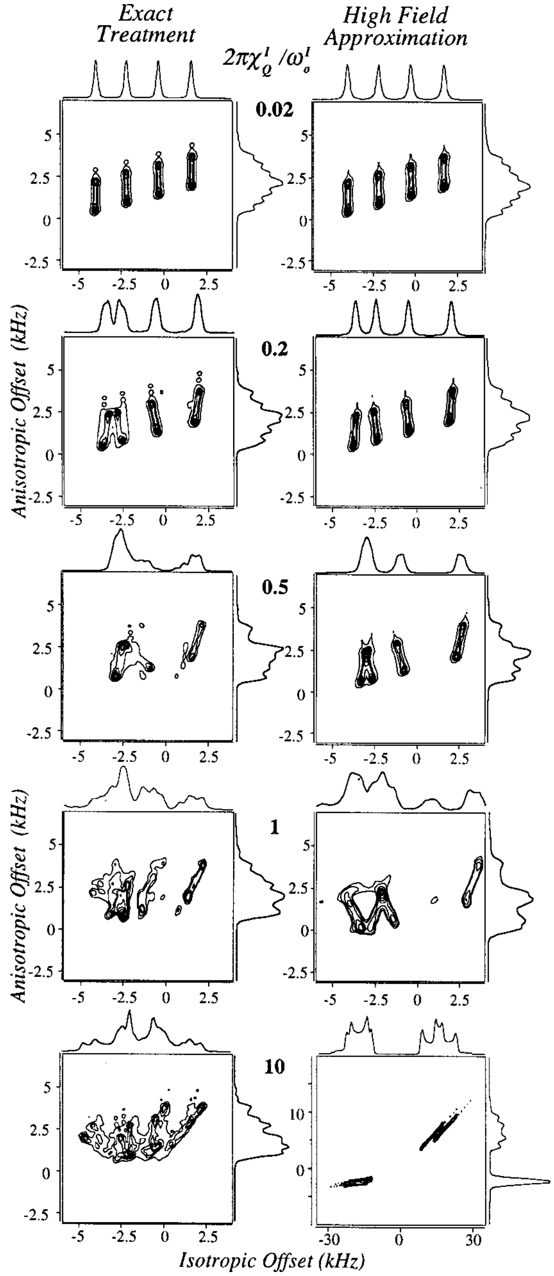

FIG. 1. Comparisons between the 2D MQMAS line shapes predicted by the exact treatment of residual dipolar couplings introduced in this study and line shapes resulting from the high field analytical expressions introduced in Ref. 18, as a function of different quadrupolar/Larmor frequency ratios. All cases assumed $S=I=3/2$, axially symmetric and coincident tensors for all interactions, MAS at $\omega_r/2\pi=25$ kHz, $J=500$ Hz, $D_{zz}^{\rm eff}=500$ Hz, $\chi_Q^S=2$ MHz, $\omega_0^S/2\pi=64.4$ MHz, $\omega_0^I/2\pi=34.4$ MHz and a natural linewidth $=50$ Hz. Vertical and horizontal traces correspond to the sheared anisotropic and isotropic 1D projections of the data. The unusual scale in the lowermost high-field simulation originates in the proportionality that this model assumes between the residual dipolar splittings and χ_Q^I.

$$\mathcal{H}_{\text{rot}}=\begin{pmatrix}
E(3/2,3/2) & 0 & 0 & 0 & \Delta^{1*}_{Q,I}+3\sqrt{3}\Gamma^{1*}_D & 0 & 0 & 0 & \Delta^{2*}_{Q,I} & 0 & 0 & 0 & 0 & 0 & 0 & 0\\
0 & E(1/2,3/2) & 0 & 0 & 0 & \Delta^{1*}_{Q,I}+\sqrt{3}\Gamma^{1*}_D & 0 & 0 & 0 & \Delta^{2*}_{Q,I} & 0 & 0 & 0 & 0 & 0 & 0\\
0 & 0 & E(-1/2,3/2) & 0 & 0 & 0 & \Delta^{1*}_{Q,I}-\sqrt{3}\Gamma^{1*}_D & 0 & 0 & 0 & \Delta^{2*}_{Q,I} & 0 & 0 & 0 & 0 & 0\\
0 & 0 & 0 & E(-3/2,3/2) & 0 & 0 & 0 & \Delta^{1*}_{Q,I}-3\sqrt{3}\Gamma^{1*}_D & 0 & 0 & 0 & \Delta^{2*}_{Q,I} & 0 & 0 & 0 & 0\\
-\Delta^{1}_{Q,I}-3\sqrt{3}\Gamma^{1}_D & 0 & 0 & 0 & E(3/2,1/2) & 0 & 0 & 0 & 6\Gamma^{1*}_D & 0 & 0 & 0 & \Delta^{2*}_{Q,I} & 0 & 0 & 0\\
0 & -\Delta^{1}_{Q,I}-\sqrt{3}\Gamma^{1}_D & 0 & 0 & 0 & E(1/2,1/2) & 0 & 0 & 0 & 2\Gamma^{1*}_D & 0 & 0 & 0 & \Delta^{2*}_{Q,I} & 0 & 0\\
0 & 0 & -\Delta^{1}_{Q,I}+\sqrt{3}\Gamma^{1}_D & 0 & 0 & 0 & E(-1/2,1/2) & 0 & 0 & 0 & -2\Gamma^{1*}_D & 0 & 0 & 0 & \Delta^{2*}_{Q,I} & 0\\
0 & 0 & 0 & -\Delta^{1}_{Q,I}+3\sqrt{3}\Gamma^{I}_D & 0 & 0 & 0 & E(-3/2,1/2) & 0 & 0 & 0 & -6\Gamma^{1*}_D & 0 & 0 & 0 & \Delta^{2*}_{Q,I}\\
\Delta^{2}_{Q,I} & 0 & 0 & 0 & -6\Gamma^{1}_D & 0 & 0 & 0 & E(3/2,-1/2) & 0 & 0 & 0 & -\Delta^{1*}_{Q,I}+3\sqrt{3}\Gamma^{1*}_D & 0 & 0 & 0\\
0 & \Delta^{2}_{Q,I} & 0 & 0 & 0 & -2\Gamma^{1}_D & 0 & 0 & 0 & E(1/2,-1/2) & 0 & 0 & 0 & -\Delta^{1*}_{Q,I}+\sqrt{3}\Gamma^{1*}_D & 0 & 0\\
0 & 0 & \Delta^{2}_{Q,I} & 0 & 0 & 0 & 2\Gamma^{1}_D & 0 & 0 & 0 & E(-1/2,-1/2) & 0 & 0 & 0 & -\Delta^{1*}_{Q,I}-\sqrt{3}\Gamma^{1*}_D & 0\\
0 & 0 & 0 & \Delta^{2}_{Q,I} & 0 & 0 & 0 & 6\Gamma^{1}_D & 0 & 0 & 0 & E(-3/2,-1/2) & 0 & 0 & 0 & -\Delta^{1*}_{Q,I}-\sqrt{3}\Gamma^{1*}_D\\
0 & 0 & 0 & 0 & \Delta^{2}_{Q,I} & 0 & 0 & 0 & \Delta^{1}_{Q,I}-3\sqrt{3}\Gamma^{1}_D & 0 & 0 & 0 & E(3/2,-3/2) & 0 & 0 & 0\\
0 & 0 & 0 & 0 & 0 & \Delta^{2}_{Q,I} & 0 & 0 & 0 & \Delta^{1}_{Q,I}-\sqrt{3}\Gamma^{1}_D & 0 & 0 & 0 & E(1/2,-3/2) & 0 & 0\\
0 & 0 & 0 & 0 & 0 & 0 & \Delta^{2}_{Q,I} & 0 & 0 & 0 & \Delta^{1}_{Q,I}+\sqrt{3}\Gamma^{1}_D & 0 & 0 & 0 & E(-1/2,-3/2) & 0\\
0 & 0 & 0 & 0 & 0 & 0 & 0 & \Delta^{2}_{Q,I} & 0 & 0 & 0 & \Delta^{1}_{Q,I}+\sqrt{3}\Gamma^{1}_D & 0 & 0 & 0 & E(-3/2,-3/2)
\end{pmatrix}. \tag{5}$$

Here

$$\begin{aligned}
E(m_S,m_I)={}&\frac{\omega_0^I}{2\pi}m_I+\chi_Q^I R_{2,0}^{Q,I}[3m_I^2-I(I+1)]+\delta_S m_S\\
&+\chi_Q^S R_{2,0}^{Q,S}[3m_S^2-S(S+1)]\\
&+\frac{6\pi(\chi_Q^S)^2}{\omega_0^S}\{R_{2,1}^{Q,S}R_{2,-1}^{Q,S}[4S(S+1)-8m_S^2-1]\\
&+R_{2,2}^{Q,S}R_{2,-2}^{Q,S}[2S(S+1)-2m_S^2-1]\}\\
&+\left(J+\sqrt{\frac{2}{3}}R_{2,0}^{D\,\text{eff}}\right)m_S m_I,\\
&-3/2\leqslant m_S,m_I\leqslant 3/2
\end{aligned} \tag{6a}$$

defines the Hamiltonian's diagonal, and off-diagonal elements are given in terms of I's laboratory frame quadrupolar couplings

$$\Delta^1_{Q,I}=3\sqrt{2}\chi_Q^I R_{2,1}^{Q,I},\quad \Delta^2_{Q,I}=3\sqrt{2}\chi_Q^I R_{2,2}^{Q,I} \tag{6b}$$

and of the dipolar coupling constant $\Gamma^1_D=R_{2,1}^{D\text{eff}}/4$.

The static central-transition NMR spectrum of the S spin could be calculated from this Hamiltonian as a suitable powder sum of the various Bohr frequencies $\nu^{(1/2)\leftrightarrow-(1/2)}(|\phi^I\rangle)=E(m_S=1/2,|\phi^I\rangle)-E(m_S=-1/2,|\phi^I\rangle)$, associated to individual I-spin eigenstates $\{|\phi^I\rangle\}$. Under MAS, however, all the anisotropic couplings in $\mathcal{H}_{\text{rot}}(\mathcal{H}_Q^I,\mathcal{H}_Q^S,\mathcal{H}_{IS})$ become time dependent. To carry out a spectral calculation one therefore needs to compute an explicit time-propagation operator

$$\begin{aligned}
U(t)&=\hat{T}\exp\left(-i\int_0^t\mathcal{H}_{\text{rot}}(t')dt'\right)\\
&=\exp[-i\mathcal{H}_{\text{rot}}(t_n)\Delta t]\times\cdots\times\exp[-i\mathcal{H}_{\text{rot}}(t_I)\Delta t]
\end{aligned} \tag{7}$$

from which the signal becomes available as

$$S(t)=\int_{\text{powder}}\text{Tr}[U(t)S_x^{(1/2)\leftrightarrow-(1/2)}U(t)^{-1}S_+^{(1/2)\leftrightarrow-(1/2)}]d\Omega. \tag{8}$$

Computing the time-dependence imparted by MAS also requires that all spatial parts of the various anisotropies be expressed in a common, rotor-based reference frame. Such transformations were defined following the conventions in Ref. 18 as

$$\begin{aligned}
&\text{EFG}(I)\xrightarrow[(a,b,c)]{}D\xrightarrow[(\alpha,\beta,\gamma)]{}\text{EFG}(S)\\
&\xrightarrow[\Omega=(\varphi,\theta,\xi)]{}\text{ROTOR}\xrightarrow[(\omega_r,54.7°,0°)]{}\text{LAB},
\end{aligned} \tag{9}$$

where the EFGs refer to the principal axes systems of the quadrupolar tensors, and arrows denote transformations based on Wigner rotations matrices.

A bi-dimensional extension of this formalism was developed to calculate the results expected from MQMAS NMR experiments. In addition to the sample spinning, this entailed correlating for every single crystallite in the sample a $m_S\leftrightarrow-m_S$ MQ evolution during a time t_1, with a conven-

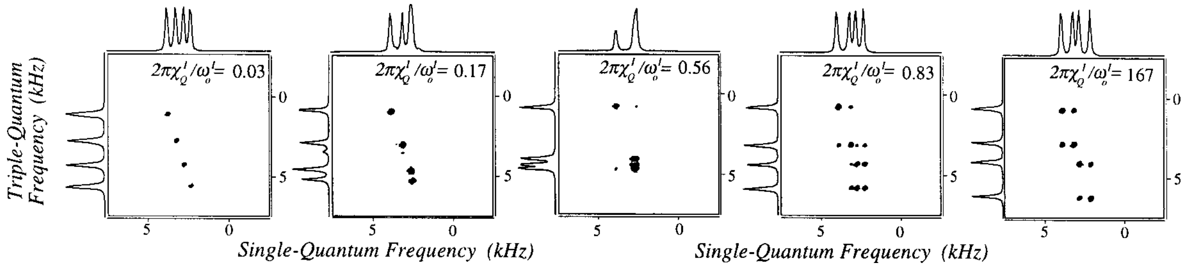

FIG. 2. Variations predicted in the triple-/single-quantum (unsheared) MAS correlation line shapes of an $I-S$ spin pair affected by residual dipolar interactions. Spectra were calculated for a single crystallite [Eq. (9) with $\varphi=0°$, $\theta=30°$] using the indicated $2\pi\chi_Q^I/\omega_0^I$ ratios, and other coupling parameters as indicated in Fig. 1.

tional $-1/2\leftrightarrow+1/2$ central transition evolution during t_2. The signal arising from the $S=3/2$ spin ensemble could then be calculated as

$$S(t_1,t_2)=\int_{\text{powder}}\text{Tr}[U(t_2)P(3Q\rightarrow 1Q)\times U(t_1)S_x^{(3/2)\leftrightarrow-(3/2)}U(t_1)^{-1}P(3Q\rightarrow 1Q)^{-1}\times U(t_2)^{-1}S_+^{(1/2)\leftrightarrow-(1/2)}]d\Omega. \tag{10}$$

Here $P(3Q\rightarrow 1Q)$ represents the unitary operator for the triple- to single-quantum conversion occurring during the mixing time, which for the sake of simplicity was assumed to have an efficiency of 100%.

In order to calculate the two-dimensional (2D) time-domain signals arising from these expressions a computer C-code program was written, involving the numerical diagonalization of the 16×16 matrix in Eq. (5) for incremented times $\Delta t_1,\Delta t_2$. Given χ_Q^I's large values, capturing with a convergent behavior the changes that occur in the $\mathcal{H}_Q^I(t)$ Hamiltonian as a result of the MAS required making these time increments significantly small ($\leqslant$1 ns). This is turn demanded thousands of diagonalizations per rotor period, a procedure that when coupled to the need for computing an untruncated bi-dimensional data set over a powdered sample became prohibitively time consuming. Because of this limitation calculations were focused on deriving an evolution operator $U(T_r)$ that is stroboscopic with the rotor period $2\pi/\omega_r$, thereby sacrificing potential spinning sideband information in exchange for computational speed. Even with this restriction the simulation of a 2D MQMAS spectrum with 23^3 powder orientations took ca. four days on a dedicated Linux-based dual-Pentium computer. Protocols based on mixed time-frequency 2D calculations as well as various algorithms for optimizing the powder averaging were assayed,[21–23] but did not result in significant improvements of the calculation's speed or on the appearance of the MQMAS line shapes.

III. RESIDUAL DIPOLAR COUPLINGS: FEATURES AND EXPERIMENTS

As an initial test of the numerical formalism we compared the 2D MQMAS NMR line shapes predicted by this approach for different values of χ_Q^I/ω_0^I, with spectra arising from the high-field analytical theory that we previously derived for this effect. Representative comparisons between these two approaches are illustrated in Fig. 1. According to these simulations the 2D correlations predicted by the analytical theory remain indistinguishable from the numerical ones for as long as $2\pi\chi_Q^I/\omega_0^I\leqslant 0.05$. Between $0.05\leqslant 2\pi\chi_Q^I/\omega_0^I\leqslant 0.2$ deviations between both sets of line shapes begin to emerge, even if the predictions that the analytical derivation makes for the centers of mass of the various $\{|\phi^I\rangle\}$ multiplet components of S remain quantitatively valid. As the $2\pi\chi_Q^I/\omega_0^I$ ratio exceeds past these values the correspondence between the high-field and the numerical predictions breaks down further, and even the number of multiplets predicted by both models for the spectra begin to differ.

In principle it may not be entirely clear whether such ''breaking apart'' of the multiplet structures is a true feature of the residual MAS dipole effects, or is reflecting a limit in the number of time and angle increments that we can adopt in the line shape simulations. Evidence that these changes are reflecting the actual spins' behavior is presented in Fig. 2, which illustrates a series of single-crystallite 2D MAS simulations obtained numerically as a function of the χ_Q^I/ω_0^I ratio. The number of orientations is not an issue in such cases, while sufficiently small Δt increments could be afforded in the propagation to guarantee a convergence in the spectral line shapes even for the highest χ_Q^I/ω_0^I ratios. These simulations confirm that simple $(2I+1)$ multiplets of the S signals will only arise in extreme high-field cases. At intermediate χ_Q^I/ω_0^I values both the number of observed peaks and their disposition becomes a complex function of the coupling parameters, a behavior that has actually been reported for the MAS NMR spectra of $S=1/2$ coupled to $I=3/2$ nuclei as well.[24] Finally in the low-field $\omega_0^I<\chi_Q^I$ regime the appearance of the 2D NMR spectrum again approaches a simple $2I+1$ multiplet when projected onto the $1Q$ or $3Q$ axes, yet it displays several cross peaks among the various S-spin components in the 2D correlation.

To further evaluate the nature of these higher-order dipolar couplings, their effects were monitored experimentally via the acquisition of solid state NMR spectra on a model ^{11}B(S)–^{75}As(I) spin pair system. The compound chosen for this test was the H_3B:$AsPh_3$ adduct, synthesized and purified as described in the literature.[25] Arsenic was chosen as coupling partner I because of several factors including its 3/2 spin number, 100% natural abundance, and relatively low Larmor frequency ($\approx\omega_0^{\text{H}}/6$). Also relevant is ^{75}As quadrupole moment (0.3×10^{-24} cm^2), that leads to large quadru-

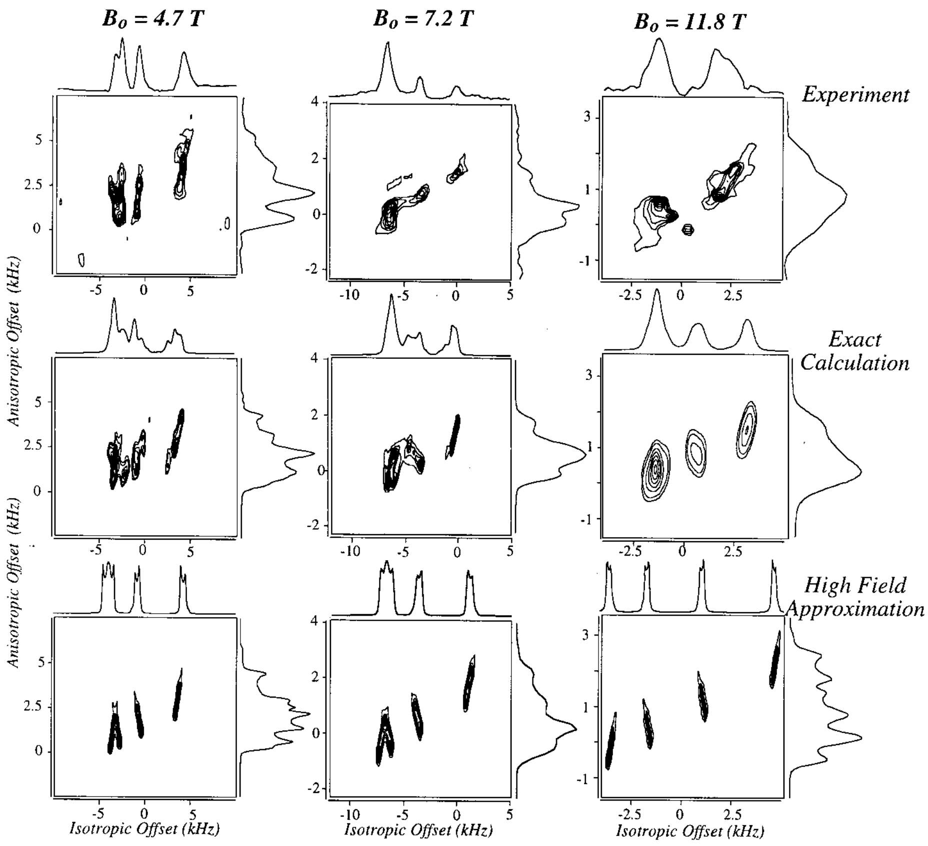

FIG. 3. Comparison between the experimental ^{11}B MQMAS centerband line shapes observed for borane triphenylarsine as a function of magnetic field (top row), and best fit simulations obtained on the basis of exact (center) and high-field (bottom) theories for the residual $S-I$ dipolar couplings. The parameters used in these calculations are $\delta_{^{11}\mathrm{B}} = -35.4$ ppm from neat $B(OCH_3)_3$; $(e^2qQ/h)_{^{11}\mathrm{B}} = 1.9$ MHz, $(e^2qQ/h)_{^{75}\mathrm{As}} = 160$ MHz, $(\eta_Q)_{^{11}\mathrm{B}} = (\eta_Q)_{^{75}\mathrm{As}} = 0$, $\Delta J = -300$ Hz, $J = 650$ Hz, natural linewidth $= 50$ Hz. Vertical and horizontal traces correspond to 1D projections of the data.

pole coupling constants in all but the most symmetric environments. ^{11}B MQMAS data were acquired for this compound on laboratory built 4.7, 7.2, and 11.8 T NMR spectrometers at 64.5, 96.8, and 160.6 MHz, respectively, using a variety of 4 and 5 mm doubly tuned probeheads while doing MAS in the 6–15 kHz range. These experiments employed a basic two-pulse MQMAS acquisition sequence with a fast-amplitude-modulation conversion pulse,[15,26,27] and relied on ≈80 kHz rf fields for both the ^{11}B manipulations and simultaneous proton decoupling.

Figure 3 displays representative variable-field 2D NMR results obtained on such compound, together with best fit simulations of these data derived using the numerical model of Sec. II. Also shown in this figure are the simulated line shapes that could have been expected from a straightforward application of the previous high-field analytical theory. In order to obtain these numerical best fit simulations, ^{11}B quadrupole coupling parameters were first extracted from the centers of mass and anisotropic projections of the variable-field MQMAS spectra. Furthermore and because of the adduct's axial symmetry along the boron-arsenic bond, the asymmetry parameter of I's EFG tensor, and the pairs of Euler angles (a,b) and (α,β) were all set to zero. This left three main parameters in control of the fit: The effective dipolar coupling, the isotropic J value, and the ^{75}As quadrupole coupling. The starting point for defining the first of these parameters was the ^{11}B–^{75}As distance reported for $H_3B{:}As(CH_3)_3$(2.03 Å);[28] further refinements demanded a decrease in the effective dipolar coupling D_{zz}^{eff}, which was arbitrarily ascribed to a lengthening of the bond by 0.2 Å (presumed to be a consequence of the more severe steric hindrance of the triphenyl arsenide) and a concurrent ΔJ anisotropy effect. The remaining values used to fit the experimental data are shown in the corresponding figure's caption. The match between all experimental and simulated spectra is not perfect, yet significant deviations of the ^{75}As quadrupole coupling constant from the reported value gave unacceptable shifts in the relative positions of the various multiplet components. It is possible that remaining discrepancies between spectra and simulations shall be reflecting nonidealities of the MQMAS sequences whose pulses were not explicitly propagated.

IV. MAS DIPOLAR EFFECTS IN THE LOW FIELD LIMIT

Although general in its applicability, the numerical approach introduced in the preceding sections is much less amenable to practical implementation than its high field analytical counterpart. The latter lead to simple expressions for the isotropic multiplet positions, and only demanded the powder integration of time-independent frequency expressions for retrieving the complete 2D MQMAS line shapes. By contrast the numerical approach provides a general description of the residual coupling at the expense of physical insight, and only gives spectral line shapes after intensive and time consuming numerical calculations that are ill-suited for iterative fittings. In an effort to alleviate this limitation, the development of a second analytical model, complementary to the existing high-field theory, was undertaken for describing the low-field case $\omega_0^I \ll \chi_Q^I$. Such treatment was derived by Olivieri for $S=1/2$ cases based on static perturbation theory;[29] this paragraph extends such model to $S=3/2$ MAS and MQMAS experiments based on an average Hamiltonian treatment.

Whereas one of the steps in the high-field analysis was a transformation to the usual Zeeman rotating frame, the low-field scenario assumes that the truncation is imposed by $\mathcal{H}_Q^I$ rather than $\mathcal{H}_Z^I$. In the corresponding quadrupolar interaction representation $\mathcal{H}_{IS}$ will assume a time dependence

$$\tilde{\mathcal{H}}_{IS}(t)=e^{i\int_0^t\mathcal{H}_Q^I(t')dt'}\mathcal{H}_{IS}e^{-i\int_0^t\mathcal{H}_Q^I(t')dt'}. \tag{11}$$

For simplicity we will consider that quadrupolar couplings χ_Q^I are time independent, and that I's quadrupolar tensor is axially symmetric and coincident with the effective dipolar PAS. Hence within this frame

$$\tilde{\mathcal{H}}_{IS}(t)=(J+D_{zz}^{\text{eff}})I_zS_z+\frac{1}{2}\left(J-\frac{D_{zz}^{\text{eff}}}{2}\right)[\tilde{I}_-(t)S_++\tilde{I}_+(t)S_-], \tag{12}$$

where

$$\tilde{I}_\pm(t)=\exp\left\{i\frac{\chi_Q^I}{\sqrt{6}}[3I_z^2-I(I+1)]t\right\}I_\pm\times\exp\left\{-i\frac{\chi_Q^I}{\sqrt{6}}[3I_z^2-I(I+1)]t\right\}. \tag{13}$$

The results of these transformations can be best expressed in terms of spherical operators,[30] which for $I=3/2$ read

$$\mp\frac{\tilde{I}_\pm(t)}{\sqrt{2}}=\tilde{T}_{1,\pm1}^I(t)=T_{1,\pm1}^I[\tfrac{3}{5}\cos(\chi_Q^It)+\tfrac{2}{5}]-\frac{i}{\sqrt{2}}T_{2,\pm1}^I\sin(\chi_Q^It)+T_{3,\pm1}^I\frac{2}{\sqrt{15}}[\cos(\chi_Q^It)-1]. \tag{14}$$

Average Hamiltonian theory can then be applied to obtain the net effect of this interaction when truncated by $\mathcal{H}_Q^I$

$$\mathcal{H}_{IS}^{(1)}=\chi_Q^I\int_0^{1/\chi_Q^I}\tilde{\mathcal{H}}_{IS}(t)dt=(J+D_{zz}^{\text{eff}})I_zS_z-\frac{1}{2}\left(J-\frac{D_{zz}^{\text{eff}}}{2}\right)\times[(I_z^2+I_z-\tfrac{3}{4})I_-S_++I_+(I_z^2+I_z-\tfrac{3}{4})S_-]. \tag{15}$$

[Having considered explicitly the modulation imposed by MAS on $\chi_Q^I(t)$ would transform all the trigonometric time dependencies in Eq. (14) into harmonic Bessel expansions, reflecting the spinning sideband pattern expected for $\mathcal{H}_Q^I(t)$. The zero-frequency components of such expansions—the centerbands for MHz-sized quadrupole couplings—have negligible intensities, thereby justifying our neglect of all the $\cos(\chi_Q t)$,$\sin(\chi_Q t)$ contributions to the average Hamiltonian $\mathcal{H}_{IS}^{(I)}$.]

Calculating the dipolar spectrum of a $-m_S\leftrightarrow+m_S$ transition involves computing differences $E_{IS}(m_S,|\phi_I\rangle)-E_{IS}(-m_S,|\phi_I\rangle)$ between $\mathcal{H}_{IS}^{(I)}$ eigenvalues

$$E_{IS}(m_S,\phi_I)=\langle\phi_{m_S}^S,\phi^I|\mathcal{H}_{IS}^{(1)}|\phi_{m_S}^S,\phi^I\rangle, \tag{16}$$

where $\{|\phi_{m_s}^S\rangle\}$ are the eigenstates of the observed spin S and $\{|\phi^I\rangle\}$ are those of the coupled spin I. For this equation to be valid both sets of eigenstates need to be expressed in the spin-space frame where the $I-S$ vector coincides with the quantization axis. For a minor Zeeman perturbation at an angle θ like the one experienced by the I spins, the quadrupolar eigenstates are given by

$$|\phi^I\rangle=\begin{cases}|3/2\rangle,\\|+\rangle=C_1|1/2\rangle+C_2|-1/2\rangle,\\|-\rangle=C_2|1/2\rangle+C_1|-1/2\rangle,\\|-3/2\rangle,\end{cases} \tag{17}$$

where

$$C_1^2+C_2^2=1$$

and

$$C_1=2\sin\theta[8-2\cos^2\theta(3+\sqrt{1+4\tan^2\theta})]^{-1/2}.$$

The S eigenstates by contrast are those of a purely Zeeman interaction, which when expressed on the dipolar PAS is given by

$$\mathcal{H}_Z^S=\omega_0^S(\cos\theta,S_z+\sin\theta S_x)=\omega_0^S\begin{pmatrix}\frac{3}{2}\cos\theta & \frac{\sqrt{3}}{2}\sin\theta & 0 & 0\\ \frac{\sqrt{3}}{2}\sin\theta & \frac{1}{2}\cos\theta & \sin\theta & 0\\ 0 & \sin\theta & -\frac{1}{2}\cos\theta & \frac{\sqrt{3}}{2}\sin\theta\\ 0 & 0 & \frac{\sqrt{3}}{2}\sin\theta & -\frac{3}{2}\cos\theta\end{pmatrix}. \tag{18}$$

This Hamiltonian is formally similar to that of an off-resonance nutation $S=3/2$ experiment. Its analytical diagonalization is outlined in the Appendix, as are the $\{|\phi_{m_S}^S\rangle\}_{-(3/2)\leqslant m_S\leqslant(3/2)}$ eigenstates to which it leads in the dipolar PAS.

With all these eigenstates at hand the dipolar frequencies affecting S's various transitions can be calculated. The result for the central $+(1/2)\leftrightarrow(1/2)$ S spectrum is

$$\nu_{IS}^{(1/2)\leftrightarrow-(1/2)}(\theta,|\phi^I\rangle)=\begin{cases}\pm\frac{3}{2}(J+D_{zz}^{\text{eff}})|\cos\theta|, & \text{for } |\phi^I\rangle=|\pm 3/2\rangle,\\ \pm\frac{1}{2}(J+D_{zz}^{\text{eff}})(C_1^2-C_2^2)\cos\theta\mp(D_{zz}^{\text{eff}}-2J)C_1C_2\sin\theta, & \text{for } |\phi^I=|\pm\rangle,\end{cases}\tag{19}$$

whereas for S's triple-quantum transitions $\nu_{IS}^{(3/2)\leftrightarrow-(3/2)}=3\,\nu_{IS}^{(1/2)\leftrightarrow-(1/2)}$. The central transition dipolar frequencies [Eq. (19)] are identical to those derived by Olivieri for a $S=1/2$;[29] consequently the remainder of the analysis can proceed along lines laid out in Ref. 29. These involve retrieving the dipolar line shapes expected upon MAS by replacing

$$\cos\theta=\cos\varepsilon\cos(54.7°)+\sin\varepsilon\sin(54.7°)\cos(\omega_r t)\tag{20}$$

into the expression for $\nu_{IS}^{m_S\leftrightarrow-m_S}(\theta,|\phi^I\rangle)$, and then integrating over a rotor cycle. The isotropic centers of mass for the various multiplets can also be calculated from an orientational averaging of the frequency expressions

$$\langle\nu_{IS}^{m_S\leftrightarrow-m_S}(|\phi^I\rangle)\rangle=\frac{1}{2}\int_0^\pi\nu_{IS}^{m_S\leftrightarrow-m_S}(\theta,|\phi^I\rangle)\sin\theta\,d\theta=\begin{cases}\pm\frac{3}{2}(J+D_{zz}^{\text{eff}})m_S & \text{for } |\phi^I\rangle=|\pm 3/2\rangle,\\ \pm(1.7092J-0.5D_{zz}^{\text{eff}})m_S & \text{for } |\phi^I\rangle=|\pm\rangle.\end{cases}\tag{21}$$

From these shiftlike MAS expressions, the centers of mass resulting from $I-S$ dipolar splittings in sheared[15] or split-t_1 (Ref. 31) MQMAS experiments become easily deduced.

It is illustrative to compare the predictions resulting from this $S=3/2$ analytical theory, with those which arise from the full numerical approach introduced in Sec. II. Figure 4 presents central transition MAS line shapes obtained numerically for various quadrupolar/Zeeman I frequency ratios, against 1D predictions expected from a suitable θ integration of Eq. (19) and from Eq. (21). The general features displayed by all these sets of spectra coincide, particularly with regards to the centers of mass exhibited by the multiplets. Yet their line shape agreement is not perfect, and gets even poorer when attempting to extend the low-field analytical formalism to the prediction of 2D MQMAS NMR line shapes.

A clue on where the disagreement between the predictions of the numerical and analytical low-field theories stems from, can be gathered from a comparison between the 2D MQMAS single-crystal spectra predicted by each model (Fig. 5, right-hand side). It becomes then clear that whereas both approaches make similar predictions for the single- and multiple-quantum 1D evolution frequencies, their 2D shapes show different cross correlations between the various sets of

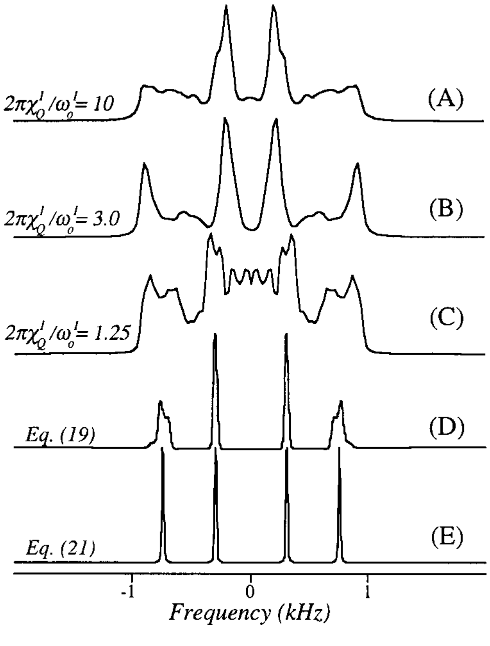

FIG. 4. Comparisons between the dipolar MAS central transition line shapes predicted by the general numeric model for different $2\pi\chi_Q^I/\omega_0^I$ ratios (A)–(C), vs the powder pattern calculated by integration of the analytical low-field expression (D). Also shown (E) is the stick spectrum predicted by the center of mass expression in Eq. (21). Spectra assumed $S=I=3/2$, $\chi_Q^S=0$, and all other parameters as in Fig. 1.

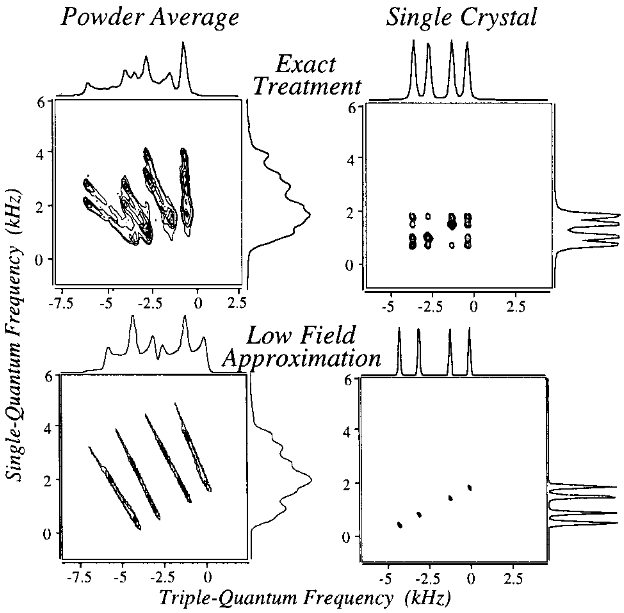

FIG. 5. Comparisons between the single-crystal (right-hand column) and powder (left-hand column) 2D triple-/single-quantum correlation line shapes predicted by the low-field analytical and by the numerical ($2\pi\chi_Q^I/\omega_0^I=100$) models. Low-field analytical spectra were built as a simple sum of $(\nu_{IS}^{(1/2)\leftrightarrow-(1/2)},\nu_{IS}^{(3/2)\leftrightarrow-(3/2)})$ cross peaks calculated from Eqs. (19)–(21); other simulations parameters are as in Fig. 1.

multiplets arising along these two axes. Indeed the analytical model associates a single S-peak component to each of the $\{|\phi_I\rangle\}$ eigenstates, whereas the density matrix simulation indicates that there is no such univocal $|\phi_I\rangle\leftrightarrow$ multiplet identity. When extended to the evaluation of powder patterns, this results in even further discrepancies between the line shapes predicted by each of the two models (Fig. 5, left-hand side). On trying to find the time-dependent $|\phi_I\rangle\leftrightarrow|\phi_I'\rangle$ transformations that would cause the multiple cross-correlation peaks displayed by the numerically derived 2D spectra, it is convenient to revisit the time-dependent changes undergone by the energy levels of the I spin. For most of the rotor period the I eigenstates are dominated by a quadrupolar Hamiltonian [Eq. (17)]; yet for a few brief instances MAS makes $\|\mathcal{H}_Q^I\|<\|\mathcal{H}_Z^I\|$, thus enabling the Zeeman perturbation to induce transitions among the various $\{|\phi^I\rangle\}$ eigenstates. Such level crossing of the I eigenstates can be considered as a laboratory frame analog of adiabatic-passage effects normally induced by rf fields in I's rotating frame, and which under proper conditions are known to induce $|\phi_I\rangle\leftrightarrow|\phi_{I'}\rangle$ transformations.[32,33] This implies that depending on the value adopted by an adiabaticity parameter $\alpha=(\omega_0^I)^2/2\pi\chi_Q^I\omega_r$, I eigenstates may interconvert or remain unchanged and thereby affect in different ways the S-spin multiplet line shape. Within the present setting, the consequence of the Zeeman-induced transitions would be the appearance of additional cross peaks among the dipolar multiplets of the S-spin 2D NMR spectrum. Such spin dynamics are not explicitly accounted for in the analytical model, solely concerned with spectral frequency calculations. Thus, depending on the particular α value, the overall appearances predicted by analytical and numerical approaches for the MQMAS spectra may or may not end up appreciably different.

V. CONCLUSIONS

This paper discussed a general treatment of the residual $I-S$ dipolar couplings that arise when heteronuclear quadrupolar spin pairs are subjected to MAS. The main emphasis was placed on the $\chi_Q^I\geqslant\omega_0^I$ regime, thereby complementing previous analytical derivations made for the $\omega_0^I\gg\chi_Q^I$ case. The result was a numerical approach that, though computationally lengthy even for the simplest $I=S=3/2$ cases, is straightforward in its implementation. Its results are novel 2D MQMAS line shapes that if appropriately analyzed can convey valuable structural and coupling information. In an effort to simplify such calculations an alternative average Hamiltonian theory was also derived, under the assumption $\omega_0^I\ll\chi_Q^I$. The resulting model yielded analytical expressions for the multiplet structures of 1D S-spin spectra which are quantitatively reliable with regards to their centers of mass, even if the complete 2D MQMAS powder line shapes may be affected by a more complex spin dynamics of the I-spin eigenstates.

ACKNOWLEDGMENTS

This work was supported by the National Science Foundation through grants DMR-9806810 and CHE-9841790 (Creativity Extension Award), as well as by the Department of Energy through Grant No. 00ER15049. L.F. is a Camille Dreyfus Teacher-Scholar, University of Illinois Junior Scholar, Alfred P. Sloan Fellow.

APPENDIX

Analytic solutions for the diagonalization of spin-3/2 Hamiltonians involving a dominant Zeeman plus a variety of other interactions (first-order quadrupolar, rf, second-order quadrupolar) have been derived in the literature.[34–36] The diagonalization of a $S=3/2$ Zeeman interaction in a tilted quantization frame appears formally similar to some of these problems but has to our knowledge not been reported. Since its results constitute an intermediate step of the calculations reported in Sec. IV, they are presented here. The eigenvalue equation $|\mathcal{H}_Z^S-\lambda I|=0$, with $\mathcal{H}_Z^S$ as in Eq. (18), leads to

$$\lambda^4-\tfrac{10}{4}(\omega_0^S)^2\lambda^2+\tfrac{9}{16}(\omega_0^S)^4=0. \tag{A1}$$

The four eigenvalues of this equation are as expected

$$\lambda_1=\frac{3\omega_0^S}{2},\quad \lambda_2=\frac{\omega_0^S}{2},\quad \lambda_3=-\frac{\omega_0^S}{2},\quad \lambda_4=-\frac{3\omega_0^S}{2}. \tag{A2}$$

The tilted eigenvectors fulfilling $\mathcal{H}_Z^S|\phi_S\rangle=\lambda_S|\phi_S\rangle$ are related to their Zeeman-based counterparts $\{|m_S\rangle\}$ by $|\phi_S\rangle=T|m_S\rangle$, where

$$T=\begin{pmatrix}
\frac{1+\cos\theta}{2}\sqrt{\frac{1+\cos\theta}{2}} & \frac{\sin\theta}{2}\sqrt{\frac{3(1+\cos\theta)}{2}} & \frac{\sin\theta}{2}\sqrt{\frac{3(1-\cos\theta)}{2}} & \frac{1-\cos\theta}{2}\sqrt{\frac{1-\cos\theta}{2}} \\
\frac{\sin\theta}{2}\sqrt{\frac{3(1+\cos\theta)}{2}} & -\frac{(3\cos\theta-1)}{2}\sqrt{\frac{1+\cos\theta}{2}} & -\frac{(3\cos\theta+1)}{2}\sqrt{\frac{1-\cos\theta}{2}} & -\frac{\sin\theta}{2}\sqrt{\frac{3(1-\cos\theta)}{2}} \\
\frac{1-\cos\theta}{2}\sqrt{\frac{3(1+\cos\theta)}{2}} & -\frac{\sin\theta(3\cos\theta+1)}{2}\sqrt{\frac{1}{2(1+\cos\theta)}} & \frac{\sin\theta(3\cos\theta-1)}{2}\sqrt{\frac{1}{2(1-\cos\theta)}} & \frac{1+\cos\theta}{2}\sqrt{\frac{3(1-\cos\theta)}{2}} \\
\frac{\sin\theta(1-\cos\theta)}{2}\sqrt{\frac{1}{2(1+\cos\theta)}} & -\frac{\sin^2\theta}{2}\sqrt{\frac{3}{2(1+\cos\theta)}} & \frac{\sin^2\theta}{2}\sqrt{\frac{3}{2(1-\cos\theta)}} & -\frac{\sin\theta(1+\cos\theta)}{2}\sqrt{\frac{1}{2(1-\cos\theta)}}
\end{pmatrix}. \tag{A3}$$

It can be confirmed that such transformation results in $\langle\phi_S|\phi_{S'}\rangle=\delta_{S,S'}$.

[1] D. Freude and J. Haase, NMR Basic Principles and Progress **29**, 1 (1993).

[2] J. Fitzgerald, *Solid State NMR of Inorganic Materials*, ACS Symp. Series 717 (American Chemical Society, Washington, DC, 1999).

[3] M. E. Smith and E. R. H. vanEck, Prog. Nucl. Magn. Reson. Spectrosc. **34**, 159 (1999).

[4] R. K. Harris and A. C. Olivieri, Prog. Nucl. Magn. Reson. Spectrosc. **24**, 435 (1992).

[5] R. K. Harris, in *Encyclopedia of NMR*, edited by D. M. Grant and R. K. Harris (Wiley, New York, 1995), p. 2909.

[6] D. L. van der Hart, H. S. Gutowsky, and T. C. Farrar, J. Am. Chem. Soc. **89**, 5056 (1967).

[7] C. J. Groombridge, R. K. Harris, K. J. Packer, B. J. Say, and S. F. Tanner, J. Chem. Soc. Chem. Commun. **1980**, 174 (1980).

[8] A. Naito, S. Ganapathy, and C. A. McDowell, J. Chem. Phys. **74**, 5393 (1981).

[9] E. M. Menger and W. S. Veeman, J. Magn. Reson. **46**, 257 (1982).

[10] J. G. Hexem, M. H. Frey, and S. J. Opella, J. Chem. Phys. **77**, 3847 (1982).

[11] A. C. Olivieri, L. Frydman, and L. E. Diaz, J. Magn. Reson. **75**, 50 (1987).

[12] A. C. Olivieri, L. Frydman, M. Grasselli, and L. E. Diaz, Magn. Reson. Chem. **26**, 615 (1988).

[13] A. C. Olivieri, J. Magn. Reson. **81**, 201 (1989).

[14] L. Frydman and J. S. Harwood, J. Am. Chem. Soc. **117**, 5367 (1995).

[15] A. Medek, J. S. Harwood, and L. Frydman, J. Am. Chem. Soc. **117**, 12779 (1995).

[16] G. Wu and K. Yamada, Chem. Phys. Lett. **313**, 519 (1999).

[17] J. McManus, R. Kemp-Harper, and S. Wimperis, Chem. Phys. Lett. **311**, 292 (1999).

[18] S. Wi and L. Frydman, J. Chem. Phys. **112**, 3248 (2000).

[19] U. Haeberlen, in *Advances in Magnetic Resonance, Suppl. 1*, edited by J. S. Waugh (Academic, New York, 1976).

[20] R. E. Wasylishen, in *Encyclopedia of Nuclear Magnetic Resonance*, edited by D. M. Grant and R. K. Harris (Wiley, New York, 1995), p. 1685.

[21] H. C. Conroy, J. Chem. Phys. **47**, 5307 (1967).

[22] M. Eden, Y. K. Lee, and M. H. Levitt, J. Magn. Reson., Ser. A **120**, 56 (1996).

[23] S. J. Varner, R. L. Vold, and G. L. Hoatson, J. Magn. Reson., Ser. A **123**, 72 (1996).

[24] S. Ding and C. A. McDowell, J. Chem. Phys. **107**, 7762 (1997).

[25] R. Goetze and H. Nöth, Z. Naturforsch. B **30**, 343 (1975).

[26] D. Massiot, B. Tonzo, D. Trumeau, J. P. Coutures, J. Virlet, P. Florian, and P. J. Grandinetti, Solid State Nucl. Magn. Reson. **6**, 73 (1996).

[27] P. K. Madhu, A. Goldbourt, L. Frydman, and S. Vega, Chem. Phys. Lett. **307**, 41 (1999).

[28] J. E. Drake, L. N. Khasrou, and A. Majid, Can. J. Chem. **59**, 2417 (1981).

[29] A. C. Olivieri, J. Magn. Reson., Ser. A **101**, 313 (1993).

[30] G. J. Bowden, W. D. Hutchison, and J. Kachan, J. Magn. Reson. **67**, 415 (1986).

[31] S. P. Brown, S. J. Heyes, and S. Wimperis, J. Magn. Reson., Ser. A **119**, 280 (1996).

[32] C. P. Grey, W. S. Veeman, and A. J. Vega, J. Chem. Phys. **98**, 7711 (1993).

[33] T. Gullion, J. Magn. Reson., Ser. A **117**, 326 (1995).

[34] R. B. Creel, J. Magn. Reson. **52**, 515 (1983).

[35] R. Jannsen and W. S. Veeman, J. Chem. Soc., Faraday Trans. 1 **84**, 3747 (1988).

[36] S. Z. Ageev and B. C. Sanctuary, Chem. Phys. Lett. **255**, 71 (1996).